

A census of transient orbital resonances encountered during binary inspiral

Uchupol Ruangsri¹ and Scott A. Hughes^{1,2,3}

¹*Department of Physics and MIT Kavli Institute,
MIT, 77 Massachusetts Ave., Cambridge, MA 02139*

²*Canadian Institute for Theoretical Astrophysics, University of Toronto,
60 St. George St., Toronto, ON M5S 3H8, Canada*

³*Perimeter Institute for Theoretical Physics, Waterloo, ON N2L 2Y5, Canada*

Transient orbital resonances have recently been identified as potentially important to the inspiral of small bodies into large black holes. These resonances occur as the inspiral evolves through moments in which two fundamental orbital frequencies, Ω_θ and Ω_r , are in a small integer ratio to one another. Previous work has demonstrated that a binary’s parameters are “kicked” each time the inspiral passes through a resonance, changing the orbit’s characteristics relative to a model that neglects resonant effects. In this paper, we use exact Kerr geodesics coupled to an accurate but approximate model of inspiral to survey orbital parameter space and estimate how commonly one encounters long-lived orbital resonances. We find that the most important resonances last for a few hundred orbital cycles at mass ratio 10^{-6} , and that resonances are almost certain to occur during the time that a large mass ratio binary would be a target of gravitational-wave observations. Resonances appear to be ubiquitous in large mass ratio inspiral, and to last long enough that they are likely to affect binary evolution in observationally important ways.

PACS numbers: 04.30.-w, 04.25.Nx, 04.70.-s

I. INTRODUCTION

A. Motivation

The evolution of large mass-ratio binaries has been a particularly active focus of research in the gravity community in recent years. This work has been motivated in part by the promise of astrophysical extreme mass ratio inspirals (or “EMRIs”) as important sources for low-frequency gravitational-wave detectors, but also because this is a limit of the general relativistic two-body problem that can in principle be solved with high precision. By treating the mass ratio of the system as a small parameter, the tools of black hole perturbation theory can be applied, treating the spacetime of the large black hole as “background,” and the effects of the smaller body as a perturbation to that background.

On short timescales, the smaller body moves on a trajectory that is nearly a geodesic orbit of the binary’s large black hole. “Nearly” refers to a *self force* arising from the small body’s interaction with its perturbation to the spacetime that pushes the small body away from the geodesic worldline; see [1, 2] for reviews of the self force research program and snapshots of recent progress. This self force has a dissipative component which is responsible for inspiral, and a conservative component which shifts the short-timescale motion with respect to geodesics. Because the motion remains close to Kerr geodesic orbits in a meaningful sense, it is useful to use geodesics as a standard against which the motion is compared.

Bound Kerr geodesics are triperiodic [3]. Each orbit has a frequency Ω_r that describes radial oscillations, a frequency Ω_θ that describes polar oscillations, and a frequency Ω_ϕ that describes rotations about the black hole’s

spin axis. In the weak field, these three frequencies become equal to one another, asymptoting to the frequency predicted by Kepler’s law. They differ significantly in the strong field, with Ω_r generically smaller than Ω_θ and Ω_ϕ . As a small body spirals into the strong-field of a large black hole, these frequencies evolve at different rates.

The different rates of evolution for these frequencies have potentially important consequences for how the self interaction affects the binary. For a slowly evolving system, each component of the self force can be written as a Fourier series in terms of the underlying fundamental frequencies [4]:

$$f^\mu = \sum_{k=-\infty}^{\infty} \sum_{n=-\infty}^{\infty} f_{kn}^\mu e^{-i(k\Omega_\theta + n\Omega_r)t}. \quad (1.1)$$

(The ϕ frequency does not enter this expansion since, by axisymmetry, the self force cannot depend on the axial position of the small body.) For a slowly evolving orbit, the Fourier components f_{kn}^μ and the frequencies themselves slowly change as the orbit proceeds. For most orbits, Eq. (1.1) indicates that the self interaction is given by a secularly evolving near-constant piece (f_{00}^μ), plus many rapidly oscillating terms (all terms with $k \neq 0$, $n \neq 0$). The rapidly oscillating terms average to zero over multiple orbits, and the bulk of the self interaction arises from f_{00}^μ .

The strong-field behavior of Kerr black hole orbits can significantly change how the self force behaves on average. Some Kerr orbits are *commensurate*: their fundamental frequencies can be written $\Omega_\theta/\Omega_r = \beta_\theta/\beta_r$, where β_θ and β_r are small integers. When this is the case, there will be a set of integers (k, n) such that

$$k\Omega_\theta + n\Omega_r = 0. \quad (1.2)$$

All terms in Eq. (1.1) for which Eq. (1.2) holds will be non-oscillatory, and so will not average away over multiple orbits. *Resonant* orbits, for which Eq. (1.2) holds for some k and n , have the potential to significantly change the evolution of binary systems near commensurate orbits as compared to the “normal” adiabatic evolution.

The importance of resonances has been the focus of several recent papers, examining their role in the astrophysics and orbital dynamics of black holes [5], the possibility that they may allow a significant speedup in the computation of radiation from Kerr orbits [6], as well as their impact on the self interaction of small bodies orbiting black holes. The first analysis looking at the self interaction was by Hinderer and Flanagan [7, 8], who developed the physical picture sketched above, and studied these systems in more detail by coupling exact Kerr geodesics to a post-Newtonian self-force model. They found that this resonant behavior near commensurate orbits can significantly change the evolution of a binary, “kicking” the evolution of the orbit’s conserved integrals as compared to an analysis that does not take the resonance into effect.

More quantitatively, let \mathcal{C} stand for one of the integrals that characterizes Kerr geodesics (the energy E , the angular momentum L_z , or the Carter constant Q). Hinderer and Flanagan show that near a resonance, the rate of change $\dot{\mathcal{C}}$ acquires a non-trivial dependence on the relative phase χ_0 of the binary’s θ and r motions. Evolving the system through resonance, one finds that \mathcal{C} is kicked by an amount $\Delta\mathcal{C}$ that depends on this phase, by the amount that $\dot{\mathcal{C}}$ differs from its average value, and by the time T_{res} that the system is “close to” the resonance:

$$\Delta\mathcal{C} = \epsilon \left[\dot{\mathcal{C}}(\chi_0) - \langle \dot{\mathcal{C}} \rangle \right] T_{\text{res}} . \quad (1.3)$$

“Close to” a resonance is defined more precisely in Sec. II B, and the phase χ_0 is defined in Sec. III A. The parameter ϵ depends in detail on how the self interaction evolves as the system moves through the resonance. The influence of these kicks in a binary’s evolution can be seen in Fig. 1 of Ref. [8] (particularly the middle panel).

B. This analysis

We now seek to go beyond the post-Newtonian approximations used in Refs. [7, 8], with the eventual goal of self consistently evolving a large mass ratio binary through resonances using a strong-field dissipative self force. As the tools to do this analysis are being developed [9], it will be useful to have some estimates of what we expect from this analysis. Our goal in this paper is to study orbital resonances using approximate tools that are simpler to use than rigorously assembling the strong-field dissipative self force.

Previous work [10] has given some insight into how self force components behave exactly on resonance, computing the on-resonance rates of change $\dot{\mathcal{C}}(\chi_0)$. Our goal

now is to begin to understand how systems behave in the vicinity of resonances. We examine a sequence of exact Kerr geodesic orbits, slowly evolving through this sequence using the Gair-Glampedakis (hereafter “GG”) “kludge” approximation [11]. Combining strong-field geodesics with the GG formulas allows us to compute sequences $[\Omega_r(t), \Omega_\theta(t)]$ which approximate those that describe a small body spiraling into a Kerr black hole in general relativity. The GG formulas are designed so that a system’s dissipation differs from rigorously computed strong-field formulas by no more than a few percent over the parameter range expected for astrophysical large-mass-ratio systems. They provide good estimates for the time it takes for a small body to spiral into a larger black hole, and should be good tools for surveying the “landscape” of orbital resonances.

The particular goal of this paper is to understand some practical issues regarding the importance of resonances: How often do resonances occur in realistic inspirals? When a resonance occurs, how long does it last? Given an ensemble of randomly selected EMRIs, how many will encounter a resonance during their inspiral, and will those resonances last long enough that they are likely to have a strong integrated effect on the system? Answering these questions will clarify how important it is to understand resonances when modeling large mass-ratio binaries. We are particularly interested in understanding this in the context of space-based low-frequency gravitational-wave observations, like the proposed eLISA mission [12]. eLISA has a nominal mission lifetime of two years. As such, resonances that occur in the final two or so years of an EMRI’s evolution are very likely to have an impact on our ability to measure their waves with this mission.

The formal answer to the question of how often resonances occur is deceptively simple: *All* EMRIs encounter an *infinite* number of resonances prior to the smaller body’s plunge into the large black hole. This is because the period associated with radial motion, T_r , diverges as the separatrix between stable and unstable orbits is approached; see Sec. III D for discussion. The period T_θ remains finite in this limit, so $\Omega_\theta/\Omega_r \rightarrow \infty$ as the separatrix is approached.

Though correct, this formal answer is not so interesting. The vast majority of those orbital resonances will be very short lived and occur in rapid succession. What is more interesting is to understand which resonances are long lived and likely to have a strong impact on the inspiral. That is the purpose of this paper.

Previous work [10] has shown that the 3:2, 2:1, and 3:1 orbital resonances are especially likely to be important — the deviation of $\dot{\mathcal{C}}(\chi_0)$ from $\langle \dot{\mathcal{C}} \rangle$ in Eq. (1.3) can be quite large, a necessary condition for the resonant parameter kick to likewise be large. In this paper, we study how often these resonances occur and how long they last for a wide range of inspirals. We pick a set of initial conditions that cover a range similar to what is expected for astrophysical EMRIs as observed by an instrument like eLISA,

and then evolve them using the GG approximation.

We find that *every* inspiral encounters at least one of these resonance during the observationally important final two years of inspiral. Many inspirals encounter two resonances, and a few encounter all three. These numbers depend strongly on binary parameters, particularly mass ratio. Setting the large black hole to mass $M = 10^6 M_\odot$ and the small one to $\mu = 1 M_\odot$, we find that the 3:1 resonance occurs in the last two years of inspiral for all the cases we have examined. The 2:1 resonance occurs during these two years if the binary’s initial orbital inclination is not too high (angle θ_{inc} , defined precisely in Sec. III A, less than about 80°), and the initial eccentricity is low ($e_{\text{init}} \lesssim 0.4$). At these masses, the 3:2 resonance does not occur during the final two years for any case we examine, although it is just slightly outside this window for very shallow ($\theta_{\text{inc}} \lesssim 10^\circ$), low eccentricity ($e_{\text{init}} \lesssim 0.4$) inspirals into rapidly spinning ($a \gtrsim 0.7M$) black holes. Because the inspiral time scales as M^2/μ , we can find cases in which all three resonances occur in the final two years if M is smaller than $10^6 M_\odot$, or μ larger than $1 M_\odot$.

In all cases, the 3:2 resonance lasts longest, meaning that the EMRI spends the most time near this resonance; the 3:1 resonance is the shortest. (“Near” resonance is defined by examining a phase variable which is stationary exactly on resonance. We define a system to be “near” resonance when this variable is within 1 radian of its value exactly on the resonance.) The fact that the 3:2 resonance lasts so long is a simple consequence of the fact that it occurs in the relative weak field (at the largest orbital radius of the resonances we survey). Conversely, the 3:1 resonance is in the relative strong field. Even the shortest resonance we survey lasts for over 50 oscillations for our $10^6:1$ binary; most of the resonances we examine last for several hundred oscillations at these masses. The number of near-resonance oscillations scales as $\sqrt{M/\mu}$, so we generically expect many dozens of oscillations even for mass ratios close to 10^5 or 10^4 .

Taken together with the on-resonance rates of change presented in Ref. [10], these results amplify the developing message of the importance of the resonant self interaction: Resonances occur frequently enough and last long enough that they are almost certain to have an important impact on the evolution of large mass-ratio binary systems. Indeed, our results imply that this behavior is generic — one should expect every observed EMRI to encounter a resonance. Self consistent modeling of a resonance’s impact on binary evolution will thus be crucial for being able to observe this systems.

The remainder of this paper is organized as follows. We begin in Sec. II with a brief overview of inspiral in EMRI systems, and of the physics of orbital resonances, highlighting what is understood today, and what remains to be clarified. In Sec. III, we describe the tools and techniques that we use here. We briefly describe our parameterization of Kerr orbits (Sec. III A) and the Gair-Glampedakis inspiral “kludge” (Sec. III B). In Sec. III C, we show how important quantities scale with the masses

of the binary’s members. This allows us to do our detailed numerical calculations for a single set of masses, and then to extrapolate from there.

Section IV presents our results. We sample a wide range of large black hole spins, a wide range of initial eccentricity e , and a wide range of initial orbit inclination θ_{inc} . We pick the initial separation so that the binary is just beyond the 3:2 resonance, and then evolve with the GG approximation until the smaller body reaches the separatrix between stable and unstable orbits. Figures 4 and 5 show our results for representative EMRIs; further data are given in Tables I – VIII. (To keep the main body of the paper from being swamped with data, these tables are given in Appendices A and B.)

Our conclusions are given in Sec. V. As already mentioned, our main conclusion is that resonances are ubiquitous and long lasting: We expect every astrophysical EMRI to encounter at least one orbital resonance en route to the binary’s final plunge, and for this resonance to last long enough that it is likely to have a substantial impact on the system’s evolution. This strongly motivates efforts to self consistently model how resonances impact extreme mass ratio binaries. We wrap up this paper by sketching plans for this analysis.

Throughout this paper, we use “relativist’s units,” with $G = 1 = c$. A useful conversion in these units is $1 M_\odot = 4.92 \times 10^{-6}$ seconds.

II. OVERVIEW: INSPIRAL AND RESONANT SELF INTERACTION

We begin with a brief overview of the self interaction and how it drives inspiral in large mass ratio binaries. We particularly highlight how the self interaction behaves near commensurate orbits, showing how to compute the quantities which will be the focus of the remainder of this paper.

A. Overview of inspiral

Consider a small body moving in the spacetime of a large black hole. The most common astrophysical motivation for this setup is the “extreme mass ratio inspiral” or EMRI, in which a compact body of mass $\mu = 1 - 100 M_\odot$ is captured onto a relativistic orbit of a black hole of mass $M = 10^{5-7} M_\odot$. We emphasize that this scenario can be taken as the large mass-ratio limit of the two-body problem in general relativity.

At zeroth order in the mass ratio, the small body follows a geodesic of the background spacetime:

$$\frac{d^2 z^\mu}{d\tau^2} + \Gamma^\mu_{\alpha\beta} \frac{dz^\alpha}{d\tau} \frac{dz^\beta}{d\tau} = 0. \quad (2.1)$$

The parameter τ is proper time along the small body’s worldline, $z^\mu(\tau)$ is its position along the worldline, and $\Gamma^\mu_{\alpha\beta}$ is the connection of the background spacetime. We

will take this background to be a Kerr black hole. The symmetries of Kerr admit a set of conserved integrals of the motion which allow us to write Eq. (2.1) as first-order equations describing motion in the four Boyer-Lindquist coordinates [13]:

$$\begin{aligned} \Sigma^2 \left(\frac{dr}{d\tau} \right)^2 &= [E(r^2 + a^2) - aL_z]^2 \\ &\quad - \Delta [r^2 + (L_z - aE)^2 + Q] \equiv R(r) , \\ \Sigma^2 \left(\frac{d\theta}{d\tau} \right)^2 &= Q - \cot^2 \theta L_z^2 - a^2 \cos^2 \theta (1 - E^2) , \end{aligned} \quad (2.2)$$

$$\Sigma \left(\frac{d\phi}{d\tau} \right) = \csc^2 \theta L_z + aE \left(\frac{r^2 + a^2}{\Delta} - 1 \right) - \frac{a^2 L_z}{\Delta} \quad (2.3)$$

$$\begin{aligned} \Sigma \left(\frac{dt}{d\tau} \right) &= E \left[\frac{(r^2 + a^2)^2}{\Delta} - a^2 \sin^2 \theta \right] \\ &\quad + aL_z \left(1 - \frac{r^2 + a^2}{\Delta} \right) . \end{aligned} \quad (2.4)$$

In these equations, $\Sigma = r^2 + a^2 \cos^2 \theta$, and $\Delta = r^2 - 2Mr + a^2$. The quantities E and L_z are the orbital energy and axial angular momentum, normalized to the mass μ of the orbiting body. They are related to the Kerr spacetime's timelike and axial Killing vectors,

$$E = -\xi_\mu^{(t)} u^\mu , \quad (2.5)$$

$$L_z = \xi_\mu^{(\phi)} u^\mu , \quad (2.6)$$

where $u^\mu \equiv dz^\mu/d\tau$ is the 4-velocity of the small body. The quantity Q is the orbit's Carter constant, normalized to μ^2 . It is related to a Killing tensor admitted by the Kerr spacetime:

$$Q = Q_{\mu\nu} u^\mu u^\nu . \quad (2.7)$$

These three quantities are conserved on any geodesic.

As described in the introduction, bound Kerr geodesics and any function which arises from them can be described in the frequency domain [3, 4] in terms of three fundamental orbital frequencies. Consider some function \mathcal{F} that depends on a bound Kerr geodesic worldline z^μ . Then, we can write

$$\mathcal{F}(z^\mu) = \sum_{mkn} \mathcal{F}_{mkn} e^{-i(m\Omega_\phi + k\Omega_\theta + n\Omega_r)t} , \quad (2.8)$$

where t is Boyer-Lindquist time. (Many functions, including the self force components we will discuss below, have no dependence on ϕ . For them, the m index can be neglected.) This expansion is very useful for describing observables such as the gravitational waves generated by a binary, since t corresponds to time as measured on the clocks of distant observers. One can also define a frequency-domain expansion like Eq. (2.8) using a time parameter that is better suited to studying the strong-field motion than t . A common choice is ‘‘Mino

time,’’ which decouples the radial and polar oscillations; see [4] for further discussion of this time parameter and the frequencies associated with it. We will use the Boyer-Lindquist time expansion (2.8) for this analysis.

At first order in the mass ratio, the spacetime is deformed by the smaller body's mass. The self interaction of the small body with its own spacetime deformation can be regarded as a *self force*¹ (or self acceleration) pushing the small body away from the geodesic worldline:

$$\frac{d^2 z^\mu}{d\tau^2} + \Gamma^\mu_{\alpha\beta} \frac{dz^\alpha}{d\tau} \frac{dz^\beta}{d\tau} = \tilde{f}^\mu . \quad (2.9)$$

Excellent discussion of the gravitational self force research program and recent progress can be found in Refs. [1, 2]. For our purposes, it is enough to note that the self force can be broken into a time-symmetric conservative piece, and a time-asymmetric dissipative piece:

$$f^\mu = f_{\text{diss}}^\mu + f_{\text{cons}}^\mu . \quad (2.10)$$

On average, the dissipative self force takes energy and angular momentum from the binary, driving the small body's inspiral, and the conservative self force shifts the orbital frequencies from their background values.

In this analysis, we neglect the conservative self force, focusing on the dissipative self interaction. We partially justify this by noting that the integrated conservative self interaction is smaller than the integrated effect of the dissipative piece by roughly the system's mass ratio [7]. We emphasize that are not arguing that it is correct to neglect the conservative self force (indeed, it is well known that the conservative self force has an important impact on the phasing of large mass ratio binaries [14]), but are just suggesting that focusing on dissipation will give insight into the astrophysical relevance of resonances.

We further justify neglecting the conservative self force for the pragmatic reason that the dissipative self force is presently better understood than the conservative one. Mature codes exist to compute the averaged effect of dissipation [15], and it appears to be straightforward to generalize these codes to analyze the instantaneous dissipative self force [9]. Detailed conservative self forces have been computed for arbitrary orbits in the Schwarzschild limit [16], and progress on the Kerr case is proceeding apace. It has already been noted using post-Newtonian techniques that the conservative self interaction has a non-negligible impact on the analysis of resonances [8, 17]. Flanagan and Hinderer in particular find for at least one example that the conservative effect, though smaller than the leading dissipative effect by about an order of magnitude, tends to augment the dissipative effects (see lower panel of Fig. 1 of Ref. [8]).

¹ The tilde on $\tilde{f}^\mu \equiv du^\mu/d\tau$ in Eq. (2.9) indicates that this describes the self interaction per unit proper time. We leave the tilde off elsewhere in this paper, indicating the self interaction per unit coordinate time: $f^\mu \equiv du^\mu/dt$.

It is not clear, though, if this is a general feature of the self force. The conservative and dissipative contributions to the self force will depend on various phases in different ways, so the augmentation that they find may be an accident of the case they focus on for their analysis. It will be valuable and interesting to include strong field conservative self forces in an analysis of this sort at some point in the future.

B. Form of the dissipative self force and its near resonant behavior

The dissipative self force has three components, which can be regarded as the instantaneous rate of change of the conserved integrals:

$$\frac{dE}{dt} = -\xi_\mu^{(t)} f_{\text{diss}}^\mu, \quad (2.11)$$

$$\frac{dL_z}{dt} = \xi_\mu^{(\phi)} f_{\text{diss}}^\mu, \quad (2.12)$$

$$\frac{dQ}{dt} = 2Q_{\mu\nu} u^\nu f_{\text{diss}}^\mu. \quad (2.13)$$

These components can be written

$$\frac{d\mathcal{C}}{dt} = \dot{\mathcal{C}}_{00} + \sum_{\substack{k=-\infty \\ k \neq 0}}^{\infty} \sum_{\substack{n=-\infty \\ n \neq 0}}^{\infty} \dot{\mathcal{C}}_{kn} e^{-i\Phi_{kn}(t)}, \quad (2.14)$$

where \mathcal{C} stands for E , L_z , or Q . We separate the 00 components to emphasize that these components survive any long-time averaging; we discuss this further below. Details of how to compute the coefficients $\dot{\mathcal{C}}_{kn}$ will be given in a forthcoming paper [9]; an example for the self force acting on a scalar charge is given in Ref. [18]. The phase variable appearing in Eq. (2.14) is given by

$$\Phi_{kn}(t) = \int_{t_0}^t [k\Omega_\theta(t') + n\Omega_r(t')] dt', \quad (2.15)$$

where t_0 is a starting time, defining when measurements of the system begin.

For most times and most index pairs (k, n) , the $e^{i\Phi_{kn}(t)}$ factor in Eq. (2.15) oscillates rapidly. When this is the case, then on average only the 00 term contributes to $d\mathcal{C}/dt$. However, if it happens that the polar and radial frequencies are *commensurate*, meaning $\Omega_\theta/\Omega_r = \beta_\theta/\beta_r$ with β_θ and β_r both integers, then the situation can change significantly. When k and n satisfy $k\beta_\theta + n\beta_r = 0$, then the phase will be *stationary* near that time, and the exponential factor in Eq. (2.15) will vary very slowly.

This behavior is illustrated in Fig. 1. We show $\cos \Phi_{kn}(t)$ for an example inspiral near a moment when $\Omega_\theta/\Omega_r = 2$; we describe how this inspiral is computed in more detail below. We have put $k = 1$ and $n = -2$, and have shifted the time axis so that $t = 0$ corresponds to the moment when $\Omega_\theta/\Omega_r = 2$. This function oscillates rapidly before and after encountering these commensurate frequencies, but varies much more slowly at times

near $t = 0$. The vertical red lines mark when $\Phi_{kn}(t)$ differs by 1 radian from its value at $t = 0$. The function oscillates rapidly outside of this window, but evolves very slowly inside.

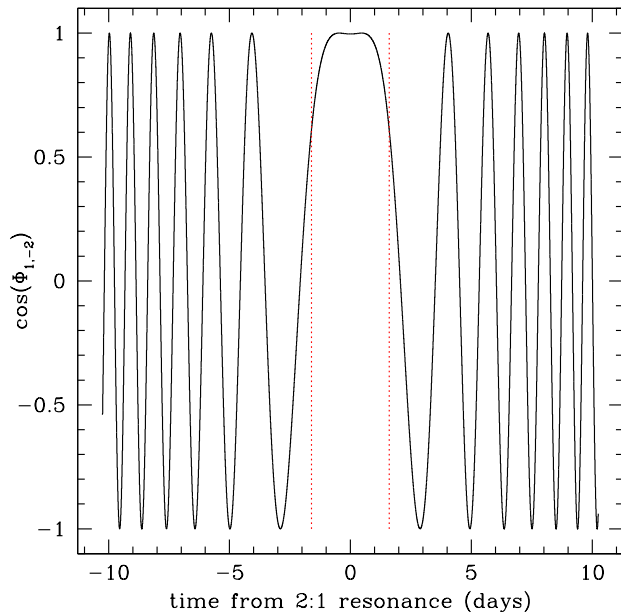


FIG. 1: Behavior of $\cos \Phi_{kn}(t)$ for $k = 1$, $n = -2$ near a moment in inspiral at which $\Omega_\theta/\Omega_r = 2$. To generate this plot, we take the large black hole to have spin $a = 0.7M$ and mass $M = 10^6 M_\odot$; the small body has mass $\mu = 1 M_\odot$. The inspiral has starting parameters $p = 7.909M$, $e = 0.4$, and $\theta_{\text{inc}} = 30^\circ$. Further data related to this case is presented in Fig. 3 and Tables III and VII.

With this behavior in mind, let us expand $\Phi_{kn}(t)$ in a Taylor series. Let t_{res} be the time at which the system encounters the resonance, and expand Φ_{kn} :

$$\begin{aligned} \Phi_{kn}(t) &= \Phi_{kn}(t_{\text{res}}) + (k\Omega_\theta + n\Omega_r)(t - t_{\text{res}}) \\ &\quad + \frac{1}{2}(k\dot{\Omega}_\theta + n\dot{\Omega}_r)(t - t_{\text{res}})^2 + \dots \\ &\simeq \Phi_{kn}(t_{\text{res}}) + \frac{1}{2}(k\dot{\Omega}_\theta + n\dot{\Omega}_r)(t - t_{\text{res}})^2. \end{aligned} \quad (2.16)$$

The frequencies and frequency derivatives here are all evaluated at t_{res} , and (k, n) are chosen so that $k\Omega_\theta + n\Omega_r = 0$ at $t = t_{\text{res}}$. Let us define the system as being “near” resonance when Φ_{kn} differs from $\Phi_{kn}(t_{\text{res}})$ by no more than one radian. By Eq. (2.16), the amount of time spent near resonance is then given by

$$T_{\text{res}} = 2\sqrt{\frac{2}{k\dot{\Omega}_\theta(t_{\text{res}}) + n\dot{\Omega}_r(t_{\text{res}})}}. \quad (2.17)$$

(The prefactor of 2 means the resonance lasts from $-T_{\text{res}}/2$ to $T_{\text{res}}/2$.) For the example shown in Fig. 1, Eq.

(2.17) predicts $T_{\text{res}} = 61170M$, within a few percent of the result $63140M$ found by directly computing the times at which the phase differs by 1 radian from $\Phi_{kn}(t_{\text{res}})$.

Multiplying T_{res} by $\Omega_{\theta,r}$, we calculate the number of orbits the system spends near resonance:

$$N_{\theta,r} = \Omega_{\theta,r} T_{\text{res}} / 2\pi. \quad (2.18)$$

We will use N_θ and N_r to describe the duration of each resonance.

III. TOOLS AND TECHNIQUES FOR OUR ANALYSIS

Here we describe the tools we use for this analysis. We discuss generic bound geodesics in Sec. III A, and the Gair-Glampedakis formulas we use to evolve through a sequence of these geodesics in Sec. III B. To reduce the number of cases we need to separately consider, we will do all of our computations for a single set of masses ($M = 10^6 M_\odot$, $\mu = 1 M_\odot$), and use the scaling laws developed in Sec. III C to extrapolate to other masses. Section III D wraps up this section by discussing the separatrix between stable and unstable orbits, and the behavior of Ω_θ/Ω_r as the separatrix is approached.

A. Generic bound geodesic orbits

The geodesic equations which describe motion at any moment have been presented in Eqs. (2.2)–(2.4). The key point for our analysis is that, up to initial conditions, geodesic motion is characterized by the three integrals E , L_z , and Q . Here, we describe in more detail how we parameterize a given orbit. We remap an orbit’s r and θ coordinates to parameters p , e , and θ_m , defined by

$$\begin{aligned} r &= \frac{pM}{1 + e \cos \psi}, \\ \cos \theta &= \cos \theta_m \cos(\chi + \chi_0). \end{aligned} \quad (3.1)$$

Strictly speaking, we should include an offset phase ψ_0 in our equation for r . For geodesics, setting $\psi_0 = 0$ amounts to choosing the time origin when the orbit passes through periapsis. For much of our analysis, we use the angle θ_{inc} introduced in Ref. [15], related to θ_m by

$$\theta_{\text{inc}} = \pi/2 - \text{sgn}(L_z) \theta_m. \quad (3.2)$$

Varying θ_{inc} from 0 to π continuously varies the orbit from prograde equatorial to retrograde equatorial. Any orbit with $\theta_{\text{inc}} < 90^\circ$ is “prograde” (L_z parallel to the black hole’s spin); any orbit with $\theta_{\text{inc}} > 90^\circ$ is “retrograde” (L_z antiparallel to the spin). Once the three parameters p , e , and θ_{inc} are known, it is straightforward to compute the three integrals E , L_z , and Q . Formulas for computing (E, L_z, Q) given $(p, e, \theta_{\text{inc}})$ can be found in Ref. [3].

References [3, 4] also provide formulas describing how to compute the three frequencies Ω_r , Ω_θ , and Ω_ϕ given p , e , and θ_{inc} . This means that, for our purposes, the parameters p , e , and θ_{inc} completely characterize Kerr black hole orbits: Once those three parameters are fixed, all other quantities describing orbits can be computed. In Ref. [10], we showed that the offset phase χ_0 is important on resonance. However, the self interaction calculations we do here are cruder than those done in Ref. [10], so we are not sensitive to χ_0 in this analysis.

B. Evolving generic generics

As already mentioned, we eventually would like to self-consistently compute the motion of the small body using a rigorously computed dissipative self force. We have begun developing code to compute the instantaneous dissipative self force components dC/dt [cf. Eq. (2.14)], and plan to couple this to a prescription for computing forced motion near Kerr black holes [19]. This work will be reported later [9].

Our goals here are more modest, so a less accurate approach to modeling the binary’s evolution will be adequate. Our main goal is simply to understand how often a given inspiral encounters an orbital resonance, and how long each resonance lasts, using Eq. (2.17) to estimate this duration. For this, we need to construct the sequence of frequencies $[\Omega_\theta(t), \Omega_r(t)]$ describing an inspiral. This can be easily done provided we likewise construct the sequence $[p(t), e(t), \theta_{\text{inc}}(t)]$, or equivalently the sequence $[E(t), L_z(t), Q(t)]$.

We use the Gair-Glampedakis (GG) “kludge” for evolving generic geodesic orbits to construct these sequences. GG provides formulas for estimating the rate at which E , L_z , and Q change due to gravitational-wave emission. By fitting to numerical results from black hole perturbation theory in the limit of zero eccentricity and zero inclination, and then using post-Newtonian results to guide their functional form, they derive formulas which fit a wide range of numerical results from black hole perturbation theory for arbitrary black hole spin, large eccentricity, and large inclination. For example, the GG formula for the rate of change of L_z is

$$\begin{aligned} \left. \frac{dL_z}{dt} \right|_{\text{GG}} &= (1 - e^2)^{3/2} \left[(1 - e^2)^{-3/2} (\dot{L}_z)_{2\text{PN}}(p, e, \iota, a) \right. \\ &\quad \left. - (\dot{L}_z)_{2\text{PN}}(p, 0, \iota, a) + (\dot{L}_z)_{\text{circ-fit}} \right]. \end{aligned} \quad (3.3)$$

This is Eq. (59) of Ref. [11]. The parameter ι is an alternate orbital inclination angle, defined by $\cos \iota = L_z / \sqrt{L_z^2 + Q}$. For Schwarzschild black holes, $\iota = \theta_{\text{inc}}$; even for maximal Kerr black holes, ι only differs from θ_{inc} by a few degrees. The function $(\dot{L}_z)_{2\text{PN}}$ is a slightly modified second post-Newtonian expression for the flux of L_z carried by gravitational waves; the function $(\dot{L}_z)_{\text{circ-fit}}$ is a (rather complicated) fit to black hole perturbation theory flux data for \dot{L}_z in the limit $e = 0$. See Secs. V and VI

of Ref. [11] [especially Eqs. (45) and (57)] for details. GG provide similar formulas to estimate dE/dt and dQ/dt .

Reference [11] demonstrates that the GG approximation provides a surprisingly good model for the inspiral of small bodies into Kerr black holes. As such, this approach is very well suited for our goal of taking a census of orbital resonances encountered during inspiral. Discussion of the resulting inspirals we make using the GG approximation is given in Sec. IV.

C. Scalings with masses

One very helpful result which is independent of our use of the GG approximation is the leading scaling of certain important quantities with the binary's masses. Consider the orbit's energy E , axial angular momentum L_z , and Carter constant Q . Recalling that we use units in which $G = c = 1$, dimensionless analogs of these quantities can be found by dividing out powers of μ and M :

$$\hat{E} = \frac{E}{\mu}, \quad \hat{L}_z = \frac{L_z}{\mu M}, \quad \hat{Q} = \frac{Q}{\mu^2 M^2}. \quad (3.4)$$

We can similarly construct dimensionless versions of the time variable t and any orbital frequency Ω_x :

$$\hat{t} = t/M, \quad \hat{\Omega}_x = M\Omega_x. \quad (3.5)$$

The leading rates of change of E , L_z , and Q have the following scalings with μ and M :

$$\frac{dE}{dt} \propto \frac{\mu^2}{M^2}, \quad (3.6)$$

$$\frac{dL_z}{dt} \propto \frac{\mu^2}{M}, \quad (3.7)$$

$$\frac{dQ}{dt} \propto \mu^3. \quad (3.8)$$

Combining Eqs. (3.6)–(3.8) with Eqs. (3.4) and (3.5), we find

$$\frac{d\hat{\mathcal{C}}}{d\hat{t}} \propto \frac{\mu}{M} \quad (3.9)$$

for $\hat{\mathcal{C}} = \hat{E}$, \hat{L}_z , and \hat{Q} . From this, we deduce how the inspiral time scales with masses: $T_{\text{insp}} \sim \mathcal{C}/(d\mathcal{C}/dt)$, so

$$T_{\text{insp}} \propto \frac{M^2}{\mu}. \quad (3.10)$$

Next we would like to understand how the duration of a resonance scales with mass ratio. Here we need the derivatives $d\Omega_{\theta,r}/dt$. The derivative of any frequency $\hat{\Omega}_x$ with \hat{t} has a very simple scaling:

$$\frac{d\hat{\Omega}_x}{d\hat{t}} = \frac{\partial\hat{\Omega}_x}{\partial\hat{E}} \frac{d\hat{E}}{d\hat{t}} + \frac{\partial\hat{\Omega}_x}{\partial\hat{L}_z} \frac{d\hat{L}_z}{d\hat{t}} + \frac{\partial\hat{\Omega}_x}{\partial\hat{Q}} \frac{d\hat{Q}}{d\hat{t}} \quad (3.11)$$

$$\propto \frac{\mu}{M}. \quad (3.12)$$

The second line follows from the fact that $\partial\hat{\Omega}_x/\partial\hat{\mathcal{C}}$ has no dependence on M or μ for $\hat{\mathcal{C}} = \hat{E}, \hat{L}_z, \hat{Q}$ — these dependences have already been scaled out at leading order. Putting factors of M and μ back in, we see that

$$\frac{d\Omega_x}{dt} \propto \frac{\mu}{M^3}. \quad (3.13)$$

By Eq. (2.17), this means that

$$T_{\text{res}} \propto \sqrt{\frac{M^3}{\mu}}, \quad (3.14)$$

and

$$N_{\theta,r} \propto \sqrt{\frac{M}{\mu}}. \quad (3.15)$$

These scalings should be accurate over the extreme mass-ratio regime. We will therefore do our calculations for only a single pair of masses ($\mu = 1 M_\odot$, $M = 10^6 M_\odot$), and extrapolate from that using these results.

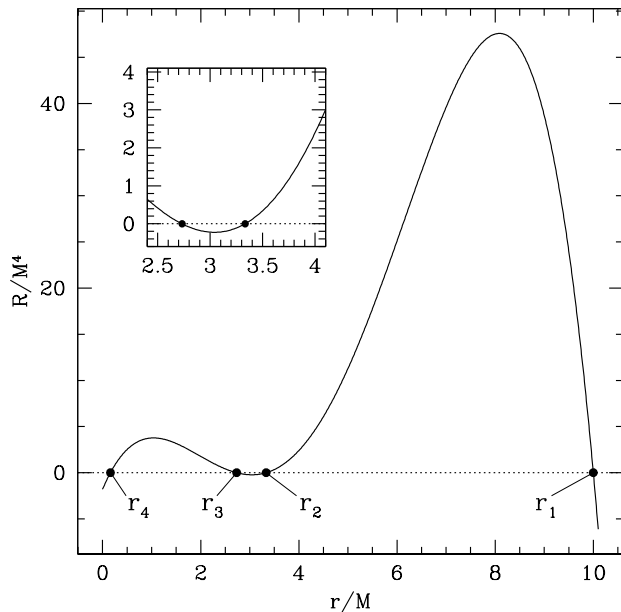


FIG. 2: Behavior of $R(r)$ for a stable orbit. This example is for an orbit about a black hole with $a = 0.7M$; it has $p = 5M$ and $e = 0.5$ (so motion is confined to $3.333M \leq r \leq 10M$), and has inclination $\theta_{\text{inc}} = 40^\circ$. The root $r_3 \simeq 2.73M$; r_1 through r_4 are indicated on the plot). As p , e , and a are held fixed and θ_{inc} increased, r_3 moves toward the orbit's periapsis, coinciding when $\theta_{\text{inc}} = 54.11^\circ$. The merging of the roots r_2 and r_3 defines the separatrix between stable and unstable orbits.

D. The stable/unstable separatrix

Coupling the GG formulas to Kerr geodesics allows us to evolve orbits under gravitational-wave emission. This

evolution drives orbits deeper into the strong field until eventually they encounter a separatrix between stable and unstable. The inspiraling body then rapidly plunges into the massive black hole. Perez-Giz and Levin [20] provide excellent discussion of the properties of this separatrix (noting that it can be understood by its equivalence to the family of Kerr spacetime homoclinic orbits), including easy-to-use formulas for computing its location in the space of bound orbits; many useful and relevant formulas can also be found in [21]. Here we briefly discuss a few critical properties of the separatrix as they pertain to our analysis.

Many of the properties of Kerr black hole orbits are determined by the function $R(r)$ defined in Eq. (2.2). It is a quartic function of Boyer-Lindquist radius r , and can be rewritten

$$R(r) = (1 - E^2)(r_1 - r)(r - r_2)(r - r_3)(r - r_4) \quad (3.16)$$

using the fact that $E < 1$ for bound orbits. The roots $r_{1,2,3,4}$ are ordered such that $r_1 \geq r_2 \geq r_3 > r_4$. They are determined by E , L_z , Q , and a ; Refs. [20, 21] provides explicit formulas for their values. Bound orbits oscillate between r_1 (apoapsis) and r_2 (periapsis), with $r_1 = r_2$ in the circular limit ($e = 0$). The root r_4 is typically inside the horizon ($r_4 = 0$ when $Q = 0$ or $a = 0$), and is never reached by any bound orbit.

Orbital stability is determined by the root r_3 . Stable bound orbits have $r_3 < r_2$; the separatrix is defined by the condition $r_3 = r_2$. Figure 2 shows $R(r)$ for one example of a stable orbit. As orbits approach the separatrix, r_3 and r_2 move together, coinciding in the limit.

Along with terminating the inspiral, the separatrix has another important property for our analysis: The radial period diverges as it is approached. This is simple to understand by analyzing the radial motion using “Mino time” λ , the time variable which separates the r and θ motions. Using λ rather than proper time τ as the independent parameter, the radial motion is governed by the equation

$$\left(\frac{dr}{d\lambda}\right)^2 = R(r). \quad (3.17)$$

The Mino-time radial period is then

$$\begin{aligned} \Lambda_r &= 2 \int_{r_2}^{r_1} \frac{dr}{\sqrt{R(r)}} \\ &= 2 \int_{r_2}^{r_1} \frac{dr}{\sqrt{(1 - E^2)(r_1 - r)(r - r_2)(r - r_3)(r - r_4)}}. \end{aligned} \quad (3.18)$$

The Boyer-Lindquist time radial period T_r is easily computed from this; see Ref. [4] for details. The key point is that $T_r \propto \Lambda_r$, and that the proportionality remains well behaved as the separatrix is approached.

At the marginally stable orbit, Eq. (3.18) becomes

$$\Lambda_r = 2 \int_{r_2}^{r_1} \frac{dr}{(r - r_2)\sqrt{(1 - E^2)(r_1 - r)(r - r_4)}}. \quad (3.19)$$

This integral, and hence Λ_r , diverges. An orbit that is precisely on the separatrix will “whirl” for all time on a circular trajectory at the orbit’s apoapsis — the hallmark of homoclinic orbits. By their proportionality, it follows that T_r also diverges as the separatrix is approached. A similar analysis shows that T_θ does *not* diverge at the separatrix, but just takes some finite value. The ratio Ω_θ/Ω_r therefore diverges on the separatrix, proving that (formally, at least) inspiraling bodies pass through an infinite number of orbital resonances en route to their final plunge into the large black hole. In practice, the small body will transition to a plunging trajectory near the separatrix.

IV. RESULTS

We now examine some key properties of extreme mass ratio systems as they evolve through resonances. We focus on two aspects of the system: How much inspiral remains after passing through a resonance; and how many oscillations in θ and r are executed near resonance.

The time remaining following each resonance is an indicator of how likely the resonance is to be of observational importance. As discussed in the Introduction, the most observationally important EMRI systems are those which are a few months or years away from their final plunge. A space-based low-frequency gravitational-wave detector like eLISA will be able to track the evolution of EMRI waves during these last few months or years. A resonance that occurs during this window is very likely to have direct observational consequences. Templates describing these systems will need to account for how the resonance modifies the binary’s “normal” adiabatic evolution in order to remain in phase with the astrophysical waveform.

The number of oscillations executed at each resonance is directly related to the “kick” imparted to the system as it evolves through resonance. We emphasize again that to build a full picture of the resonance’s impact we must self-consistently integrate the system under the influence of the dissipative self force, which we plan to do in future work [9]. However, in the absence of this self-consistent picture, we can say with confidence that longer resonances are likely to imply greater “kicks” to orbital parameters, and vice versa. The duration of a resonance is thus an important indicator of its possible importance in the evolution of an EMRI.

Before discussing our results in detail, we first describe how we select the different inspirals that we study. Our goal is to cover a range of parameters which span what is likely for astrophysical EMRI events that may be measured by a future low-frequency GW mission, while keeping the total number of cases we study reasonable. The algorithm we follow is as follows:

- Choose the large black hole’s spin from the set $a/M \in [0.1, 0.4, 0.7, 0.9]$. This range nicely covers the possibilities from slow to rapid spin.

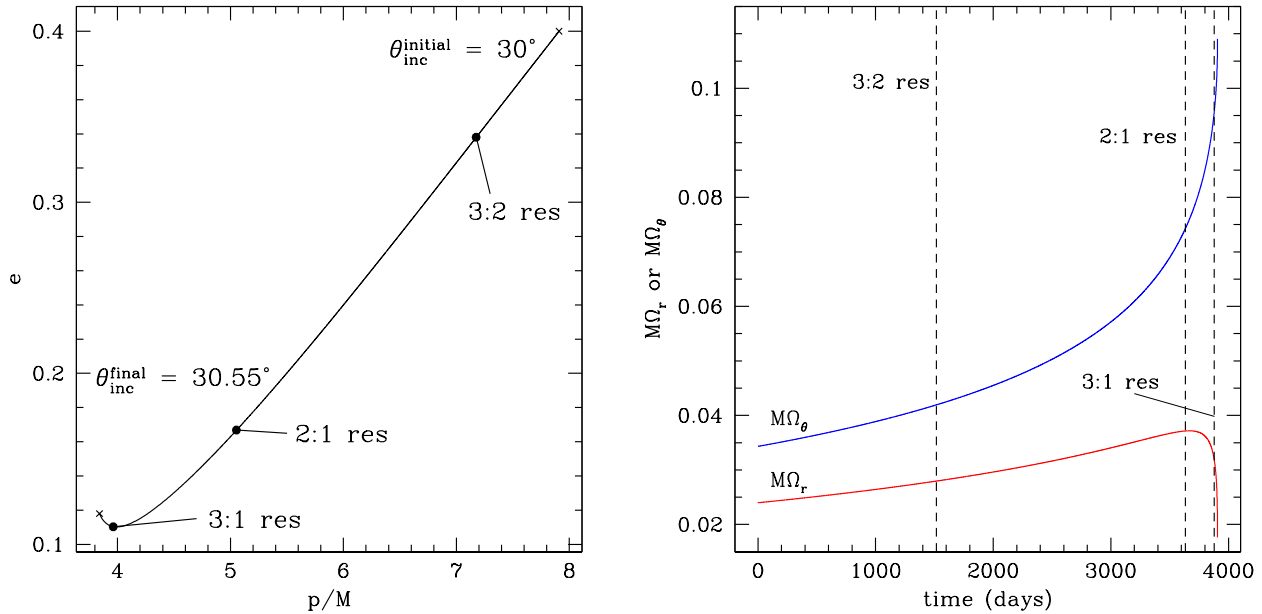


FIG. 3: Behavior of important quantities describing an inspiral in the GG approximation; the case shown here is the same one used to generate Fig. 1. Left panel shows the evolution of p , e , and θ_{inc} . Inspirals starts at the upper right cross, and ends at the lower left cross. During evolution, p shrinks until the system reaches the separatrix; e mostly shrinks over inspiral, growing for a short time near the end. The inclination angle θ_{inc} is nearly constant over inspiral, increasing by about half a degree. The three dots on the track mark the moments that the binary passes through the resonances we study. Right panel shows the evolution of Ω_r and Ω_θ as functions of time. Dashed vertical lines mark the resonances. We have done these calculations with masses $M = 10^6 M_\odot$, $\mu = 1 M_\odot$. To extrapolate to other masses, use the fact that the time axis scales as M^2/μ , and that all other quantities shown here are invariant to mass scaling.

- Pick initial orbital eccentricity from the set $e \in [0.1, 0.4, 0.7, 0.95]$. This set covers a large portion of the range that is likely to describe astrophysical EMRI events [23].
- Pick initial orbital inclination from the set $\theta_{\text{inc}} \in [10^\circ, 30^\circ, 60^\circ, 85^\circ, 95^\circ, 120^\circ, 150^\circ, 170^\circ]$. This set surveys a range from nearly prograde equatorial orbits to nearly retrograde equatorial orbits. We are careful not to examine orbits precisely at 90° , since the GG approximation may not be reliable there. Because θ_{inc} evolves only slightly [11, 22], its value is nearly fixed to its initial value over inspiral.
- Compute the value of p so that an orbit is exactly on the 3:2 resonance. We then inflate that value by 10%, and allow the binary to evolve using the GG approximation (Sec. III B).

In all cases, we fix the binary’s masses to $M = 10^6 M_\odot$, $\mu = 1 M_\odot$, and extrapolate to other masses using the results of Sec. III C.

Figure 3 shows an example binary selected by this procedure and then evolved with the GG approximation. The large black hole has $a = 0.7M$, and the binary begins with $e = 0.4$, $\theta_{\text{inc}} = 30^\circ$. (These are the parameters used to illustrate the near resonance stationary phase of the self interaction in Fig. 1.) Left panel shows how the

binary evolves across the (p, e) plane — shrinking in p over the entire inspiral, shrinking in e until very late in the inspiral, and with θ_{inc} nearly constant. Notice that as the binary crosses the three orbital resonances that we study, p and e are smaller (in some cases, significantly smaller) than their starting values. The right panel shows how the binary’s frequencies Ω_θ and Ω_r evolve with time, with vertical dashed lines labeling the moments that the system passes through orbital resonances.

Although differing in detail, all of the examples we study are qualitatively similar to this case. In particular, we always find that p shrinks over the entire inspiral; e shrinks until the very end, at which point it grows slightly. (This behavior was originally discovered in studies of eccentric orbits spiralling into non-rotating black holes [24], and was later confirmed to hold for all spins [25].) The frequency Ω_θ grows monotonically over the inspiral; Ω_r reaches a maximum in the strong field, but then turns over, approaching 0 near the separatrix (cf. Sec. III D).

Figure 4 shows how much time remains following each resonance for the binary shown in Fig. 3. For the masses used to generate this plot, the 3:1 resonance occurs in the last several months of resonance at all inclinations; the 2:1 resonance occurs in the final two years of inspiral at inclinations less than about 80° . The 3:2 resonance occurs much earlier (nearly six years before plunge at

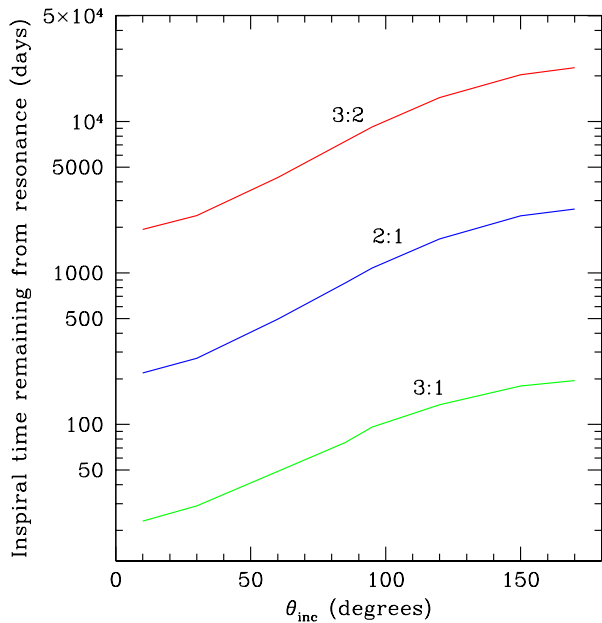


FIG. 4: Inspirational time remaining following resonance passage as a function of initial θ_{inc} for $a = 0.7M$, initial $e = 0.4$. These numbers assume $M = 10^6 M_\odot$, $\mu = 1 M_\odot$; Using $T_{\text{insp}} \propto M^2/\mu$ [Eq. (3.10)], it is simple to extrapolate to other masses. Red curve shows the time remaining for the 3:2 resonance, blue for the 2:1 resonance, and green for 3:1. Similar results can be found for other choices of black hole spin and initial eccentricity; see Tables I – IV for detailed data.

the largest inclination we examine). Bearing in mind the M^2/μ scaling of inspiral time, this plot indicates that the 3:1 resonance occurs during the final two years of inspiral for essentially all astrophysically important EMRIs. In many cases, both the 2:1 and 3:1 resonances occur during this time period. For shallow inclination and somewhat less extreme mass ratio (e.g., $M = 10^6 M_\odot$, $\mu = 10 M_\odot$), all three of the resonances we have examined occur during the final two years of EMRI evolution.

Data describing inspiral for other values of spin and eccentricity is presented in Tables I – IV, in Appendix A. Although differing in detail, their qualitative form is broadly the same as that shown in Fig. 4. In particular, for $M = 10^6 M_\odot$, $\mu = 1 M_\odot$, the 3:1 resonance occurs in the last few months of inspiral nearly always, reaching to about a year before final plunge in the most extreme cases; the 2:1 resonance occurs during the last two years for shallow orbital inclinations and relatively small initial eccentricities; and the 3:2 resonance occurs several years from final plunge. All three resonances are likely to occur in the last few years if the smaller mass is $10 M_\odot$ or larger, or if the larger mass is smaller than $10^6 M_\odot$.

Figure 5 shows how many radial oscillations N_r the system executes as it passes through each resonance, using Eq. (2.18); N_θ is simply related to N_r by the resonance number. Computations are again done for the $a = 0.7M$, $e_{\text{init}} = 0.4$ system that was used to generate Figs. 1, 3,

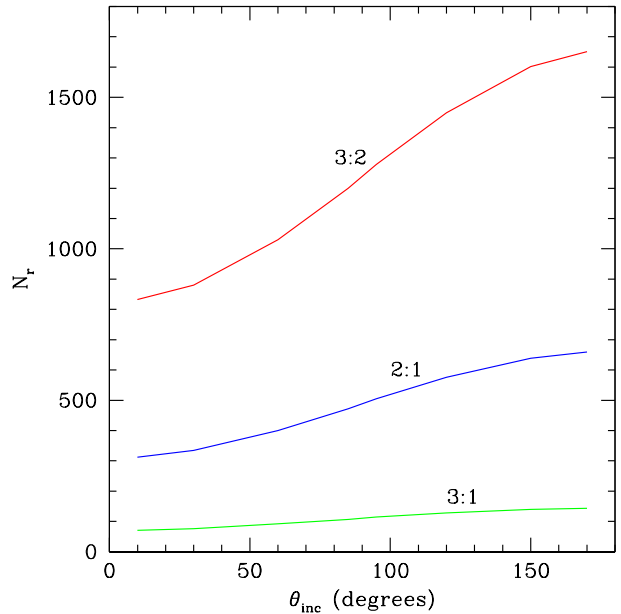


FIG. 5: Number of orbits N_r near resonance [defined by Eq. (2.18)] as a function of initial θ_{inc} for $a = 0.7M$, initial $e = 0.4$. These numbers assume $M = 10^6 M_\odot$, $\mu = 1 M_\odot$; using the rule that $N_r \propto \sqrt{M/\mu}$ [Eq. (3.15)], it is simple to extrapolate to other masses. (The number of θ oscillations is simply related to the number of r oscillations by the resonance number.) The results are similar for other choices of black hole spin and initial orbital eccentricity.

and 4. Data describing other cases can be found in Tables V – VIII in Appendix B. In all cases, the results are qualitatively quite similar to Fig. 5, though differing in quantitative detail.

It's worth noting that both the duration of each resonance and the amount of inspiral left following resonance passage depend in a very simple way on a single parameter — the value of semi-latus rectum p at the moment of resonance passage. When a resonance occurs at large p , EMRI systems evolve relatively slowly, and they spend more time near resonances. The converse holds when resonances occur at small p . We show this in Fig. 6, which is the same data as that shown in Fig. 5, but rearranged to show N_r as a function of $p_{\beta_\theta:\beta_r}$, the semi-latus rectum at the moment of resonance passage. Note that N_r is close to a linear function of $p_{\beta_\theta:\beta_r}$. This is consistent with the results of Ref. [5], which shows that eccentricity has only a modest effect on the value of p at which a resonance occurs except for orbits that are very close to the separatrix. A similar figure could be made to show how the time remaining in inspiral depends on $p_{\beta_\theta:\beta_r}$.

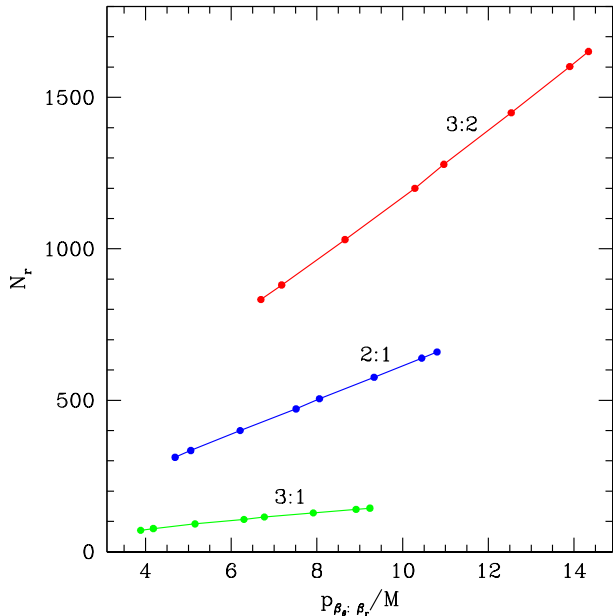


FIG. 6: Reorganization of the data shown in Fig. 5: We now show the number of orbits near resonance as a function of semi-latus rectum p at resonance passage. The points on each track label the different inclinations we study; from left to right, they are $\theta_{\text{inc}} = 10^\circ, 30^\circ, 60^\circ, 85^\circ, 95^\circ, 120^\circ, 150^\circ$, and 170° . Notice the nearly linear dependence of N_r on p .

V. CONCLUSIONS

Taken together, Figs. 4 and 5 (and their counterparts in Tables I – VIII) present the main message of this paper: Orbital resonances are ubiquitous in extreme mass ratio inspiral, and each resonance lasts for many oscillations — several dozen to many hundred, depending on the system’s mass ratio. This amplifies the developing message of ongoing work on resonances: These effects are likely to have an observationally important effect on astrophysical extreme mass ratio systems.

It is worth noting that, in addition to the issues we consider here and in associated analyses, many other factors have an impact on the astrophysical relevance of resonances. Among them² are: The lifetime of the eLISA mission (or whatever low-frequency GW mission eventually measures EMRI waves); what portion of the EMRI signals overlap in time with this mission; the strength of the waves, and hence the integrated signal-to-noise ratio (especially the contribution to the signal-to-noise ratio from resonances); and the EMRI event rate, both in total, and as distributed with the masses M and μ . These points are, by and large, not well understood; and they

² We thank this paper’s referee for reminding us that the following points are also important, and should be emphasized.

are rather coupled to one another. We will not pretend to offer any deep wisdom, but will simply note that as the community begins to think about the impact that resonances can have upon EMRI measurements, these points must be considered eventually as well.

Although we have now studied various pieces of what is needed to understand the resonant evolution of extreme mass ratio binaries, it remains necessary that they be assembled in a self-consistent manner. Roughly speaking, the results of this paper tell us the “width” of each resonance (i.e., the time in which a system’s evolution is substantially modified by resonant physics); those of Ref. [10] tell us the each resonance’s “height” (i.e., the extent of the deviation of the on-resonance rate of change of system parameters). Up to a factor of order unity, the product of these numbers tells us the kick in the binary’s parameters due to evolving through an orbital resonance (cf. Fig. 1 of Ref. [8]).

It is satisfying that our results are, so far, consistent with the picture originally developed by Flanagan and Hinderer [8]. However, rough agreement is not good enough for modeling EMRI systems. More precise understanding of how a system evolves through orbital resonances is almost certainly necessary to ensure that future observatories like eLISA will be able to measure these waves. Our plan for going beyond this analysis is to compute components of the instantaneous dissipative self force and the self consistently evolve the system as a “forced geodesic” [19]. Results describing the instantaneous dissipative self force for scalar fields are given in Ref. [18]; generalizing to the gravitational interaction is straightforward provided we focus on the dissipative contribution. It turns out that all of the quantities we need can be computed with relatively minor modifications of pre-existing Teukolsky-equation solvers [15, 22]. As an example, one component of the dissipative self force can be written as the rate of change of orbital energy per unit Mino time λ [9, 26]:

$$\frac{dE}{d\lambda} = \sum_{k'n'} \mathcal{E}_{k'n'} e^{-i(k'\Upsilon_\theta + n'\Upsilon_r)\lambda}, \quad (5.1)$$

where $\Upsilon_{\theta,r}$ are orbital frequencies conjugate to Mino-time λ , and where

$$\mathcal{E}_{k'n'} = \sum_{lmkn} \frac{\Gamma}{4\pi\omega_{mkn}^2} Z_{lmkn} Z_{lm(k+k')(n+n')}^*. \quad (5.2)$$

The amplitudes Z_{lmkn} describe the amplitude of the curvature scalar ψ_4 in a harmonic and Fourier decomposition; superscript $*$ denotes complex conjugation, Γ relates Mino-time λ to Boyer-Lindquist time t , and ω_{mkn} is a mode frequency conjugate to t .

The self force is of course gauge dependent; however, a two-timescale analysis [7] shows that its impact over a long timescale T_{insp} is dominated by a gauge-independent result (with subleading gauge-dependent contributions that scale as $T_{\text{orb}}/T_{\text{insp}}$). Hence the results computed

in this way are not gauge ambiguous provided we integrate the system over a long time compared to a typical orbital period. We are now beginning to overhaul our group's Teukolsky equation codebase in order to do this analysis.

Acknowledgments

This paper originated in a question Eric Poisson asked of SAH about whether resonances occur in realistic inspirals, or whether they are rare curiosities; we thank him for motivating us to thoroughly examine and answer this question. We gratefully acknowledge many useful discussions on the subject of resonances in extreme mass ratio inspiral with Éanna Flanagan, Tanja Hinderer, and Gabriel Perez-Giz, and we thank this paper's referee for making several helpful suggestions. This work was supported by NSF Grant PHY-1068720. SAH gratefully acknowledges fellowship support by the John

Simon Guggenheim Memorial Foundation, and sabbatical support from the Canadian Institute for Theoretical Astrophysics and the Perimeter Institute for Theoretical Physics.

Appendix A: Inspiral time remaining following resonance passage

In this appendix, we present detailed data showing how the inspiral time remaining following resonance passage depends on EMRI parameters.

Appendix B: Detailed tables describing duration of each resonance

In this appendix, we present detailed data showing how the duration of each resonance depends on EMRI parameters.

-
- [1] E. Poisson, A. Pound, and I. Vega, *Liv. Rev. Rel.* **14**, 7 (2011).
 - [2] L. Barack, *Class. Quantum Grav.* **26**, 213001 (2009).
 - [3] W. Schmidt, *Class. Quantum Grav.* **19**, 2743 (2002).
 - [4] S. Drasco and S. A. Hughes, *Phys. Rev. D* **69**, 044015 (2004).
 - [5] J. Brink, M. Geyer, and T. Hinderer, arXiv:1304.0330.
 - [6] R. Grossman, J. Levin, and G. Perez-Giz, *Phys. Rev. D*, submitted; arXiv:1108.1819.
 - [7] T. Hinderer and E. E. Flanagan, *Phys. Rev. D* **78**, 064028 (2008).
 - [8] E. E. Flanagan and T. Hinderer, *Phys. Rev. Lett.* **109**, 071102 (2012).
 - [9] E. E. Flanagan, T. Hinderer, S. A. Hughes, and U. Ruangsri, in preparation.
 - [10] E. E. Flanagan, S. A. Hughes, and U. Ruangsri, *Phys. Rev. D*, submitted; arXiv:1208.3906.
 - [11] J. R. Gair and K. Glampedakis, *Phys. Rev. D* **73**, 064037 (2006).
 - [12] P. Amaro Seone et al., *The Gravitational Universe*, white paper submitted to the European Space Agency's Cosmic Vision program; astro-ph/1305.5720.
 - [13] C. W. Misner, K. S. Thorne, and J. A. Wheeler, *Gravitation* (Freeman, San Francisco, 1973).
 - [14] A. Pound, E. Poisson, and B. G. Nickel, *Phys. Rev. D* **72**, 124001 (2005).
 - [15] S. Drasco and S. A. Hughes, *Phys. Rev. D* **73**, 024027 (2006).
 - [16] L. Barack and N. Sago, *Phys. Rev. D* **81**, 084021 (2010).
 - [17] S. Isoyama, R. Fujita, H. Nakano, N. Sago, and T. Tanaka, *Prog. Theor. Exp. Phys.* 063E01 (2013).
 - [18] S. Drasco, E. E. Flanagan, and S. A. Hughes, *Class. Quantum Grav.* **22**, S801 (2005).
 - [19] J. R. Gair, E. E. Flanagan, S. Drasco, T. Hinderer, and S. Babak, *Phys. Rev. D* **84**, 044037 (2011).
 - [20] G. Perez-Giz and J. Levin, *Phys. Rev. D* **79**, 123013 (2009).
 - [21] R. Fujita and W. Hikida, *Class. Quantum Grav.* **26**, 135002 (2009).
 - [22] S. A. Hughes, *Phys. Rev. D* **61**, 084004 (2000).
 - [23] J. R. Gair, L. Barack, T. Creighton, C. Cutler, S. L. Larson, E. S. Phinney, and M. Vallisneri, *Class. Quantum Grav.* **21**, S1595 (2004).
 - [24] C. Cutler, D. Kennefick, and E. Poisson, *Phys. Rev. D* **50**, 3816 (1994).
 - [25] K. Glampedakis and D. Kennefick, *Phys. Rev. D* **66**, 044002 (2002).
 - [26] E. E. Flanagan and T. Hinderer, private communication.

p_{init}/M	e_{init}	$\theta_{\text{inc, init}}$	$p_{3:2}/M$	$e_{3:2}$	$T_{3:2}$ (days)	$p_{2:1}/M$	$e_{2:1}$	$T_{2:1}$ (days)	$p_{3:1}/M$	$e_{3:1}$	$T_{3:1}$ (days)
11.297	0.1	10°	10.270	0.085	6888	7.580	0.053	854	6.390	0.045	97
11.363	0.1	30°	10.334	0.085	7032	7.630	0.053	872	6.433	0.045	99
11.583	0.1	60°	10.531	0.085	7489	7.786	0.053	930	6.566	0.046	105
11.825	0.1	85°	10.753	0.086	8029	7.961	0.054	999	6.718	0.046	113
11.935	0.1	95°	10.846	0.085	8265	8.035	0.054	1029	6.781	0.046	116
12.177	0.1	120°	11.067	0.086	8844	8.210	0.054	1103	6.933	0.047	125
12.397	0.1	150°	11.263	0.086	9379	8.366	0.054	1171	7.067	0.047	132
12.463	0.1	170°	11.326	0.086	9557	8.416	0.055	1194	7.111	0.048	134
11.385	0.4	10°	10.332	0.346	7417	7.624	0.220	858	6.460	0.189	71
11.451	0.4	30°	10.396	0.346	7571	7.674	0.220	876	6.504	0.190	72
11.671	0.4	60°	10.593	0.346	8057	7.831	0.222	933	6.640	0.192	76
11.913	0.4	85°	10.815	0.347	8628	8.007	0.224	999	6.795	0.195	81
12.034	0.4	95°	10.909	0.346	8889	8.081	0.223	1031	6.858	0.194	84
12.276	0.4	120°	11.130	0.346	9500	8.258	0.225	1101	7.013	0.197	88
12.485	0.4	150°	11.326	0.347	10072	8.414	0.227	1167	7.151	0.200	93
12.562	0.4	170°	11.389	0.346	10260	8.465	0.227	1189	7.195	0.200	94
11.572	0.7	10°	10.473	0.618	9588	7.742	0.419	929	6.648	0.370	49
11.649	0.7	30°	10.537	0.618	9775	7.794	0.420	947	6.693	0.371	49
11.869	0.7	60°	10.734	0.618	10390	7.952	0.422	1006	6.834	0.375	52
12.111	0.7	85°	10.957	0.618	11108	8.131	0.426	1071	6.996	0.380	53
12.221	0.7	95°	11.051	0.618	11460	8.205	0.424	1110	7.059	0.378	56
12.474	0.7	120°	11.273	0.618	12218	8.384	0.427	1179	7.221	0.383	58
12.683	0.7	150°	11.470	0.618	12956	8.543	0.430	1248	7.365	0.387	61
12.760	0.7	170°	11.533	0.618	13189	8.594	0.430	1270	7.411	0.388	62
11.803	0.95	10°	10.651	0.853	18801	7.926	0.622	1139	6.933	0.569	35
11.880	0.95	30°	10.715	0.852	19128	7.978	0.622	1160	6.979	0.570	36
12.100	0.95	60°	10.913	0.852	20320	8.138	0.624	1230	7.125	0.574	37
12.342	0.95	85°	11.137	0.853	21773	8.320	0.629	1308	7.294	0.580	39
12.452	0.95	95°	11.230	0.852	22396	8.393	0.626	1359	7.356	0.577	41
12.705	0.95	120°	11.453	0.852	23851	8.575	0.630	1441	7.524	0.582	42
12.925	0.95	150°	11.651	0.852	25264	8.736	0.632	1524	7.672	0.586	44
12.991	0.95	170°	11.715	0.852	25793	8.789	0.633	1552	7.720	0.587	45

TABLE I: Various characteristics of inspirals that encounter the 3:2, 2:1, and 3:1 orbital resonances. We show the values of p , e , and θ_{inc} at the beginning of each inspiral, and the values of p , e , and the time remaining in the inspiral at each resonance crossing. (The inclination θ_{inc} barely changes during inspiral, so we do not show those data.) In all cases, the large black hole's spin is $a = 0.1M$; the binary's masses are $M = 10^6 M_{\odot}$, $\mu = 1 M_{\odot}$. The times can be extrapolated to other masses using the rule that $T_{\text{insp}} \propto M^2/\mu$ [Eq. (3.10)]. Notice that significant inspiral remains following each resonance.

p_{init}/M	e_{init}	$\theta_{\text{inc, init}}$	$p_{3:2}/M$	$e_{3:2}$	$T_{3:2}$ (days)	$p_{2:1}/M$	$e_{2:1}$	$T_{2:1}$ (days)	$p_{3:1}/M$	$e_{3:1}$	$T_{3:1}$ (days)
9.427	0.1	10°	8.574	0.084	3844	6.229	0.048	468	5.223	0.038	54
9.713	0.1	30°	8.836	0.085	4240	6.432	0.048	518	5.393	0.039	59
10.604	0.1	60°	9.642	0.085	5642	7.061	0.050	694	5.926	0.042	79
11.594	0.1	85°	10.542	0.085	7575	7.772	0.053	939	6.538	0.045	106
12.012	0.1	95°	10.919	0.085	8519	8.072	0.053	1060	6.797	0.045	120
12.991	0.1	120°	11.805	0.086	11063	8.781	0.055	1386	7.414	0.048	156
13.849	0.1	150°	12.582	0.086	13721	9.406	0.056	1729	7.961	0.050	194
14.124	0.1	170°	12.832	0.086	14670	9.608	0.057	1851	8.138	0.051	207
9.515	0.4	10°	8.632	0.343	4166	6.263	0.200	482	5.269	0.161	46
9.801	0.4	30°	8.894	0.343	4584	6.467	0.203	529	5.441	0.165	48
10.681	0.4	60°	9.699	0.345	6071	7.099	0.212	703	5.983	0.177	61
11.671	0.4	85°	10.601	0.347	8108	7.816	0.221	938	6.608	0.191	77
12.100	0.4	95°	10.978	0.346	9157	8.116	0.221	1067	6.868	0.189	90
13.079	0.4	120°	11.867	0.347	11851	8.830	0.229	1378	7.500	0.202	110
13.937	0.4	150°	12.647	0.348	14688	9.459	0.234	1709	8.059	0.210	132
14.223	0.4	170°	12.898	0.348	15699	9.663	0.235	1826	8.241	0.212	139
9.702	0.7	10°	8.764	0.614	5419	6.360	0.388	536	5.400	0.321	34
9.977	0.7	30°	9.026	0.616	5954	6.566	0.393	589	5.580	0.329	37
10.868	0.7	60°	9.830	0.617	7812	7.205	0.406	768	6.142	0.349	45
11.858	0.7	85°	10.734	0.619	10355	7.932	0.423	1002	6.796	0.375	53
12.287	0.7	95°	11.112	0.617	11767	8.232	0.419	1155	7.055	0.369	62
13.266	0.7	120°	12.007	0.619	15178	8.959	0.433	1468	7.719	0.391	72
14.135	0.7	150°	12.792	0.620	18807	9.599	0.441	1804	8.303	0.403	83
14.421	0.7	170°	13.046	0.620	20100	9.806	0.443	1925	8.493	0.407	87
9.911	0.95	10°	8.935	0.851	10636	6.523	0.591	671	5.636	0.516	26
10.197	0.95	30°	9.195	0.851	11629	6.730	0.596	730	5.820	0.524	28
11.077	0.95	60°	9.998	0.852	15228	7.374	0.609	940	6.400	0.547	33
12.078	0.95	85°	10.903	0.854	20178	8.111	0.627	1208	7.081	0.576	38
12.507	0.95	95°	11.283	0.851	22794	8.410	0.620	1416	7.336	0.564	47
13.497	0.95	120°	12.183	0.853	29589	9.150	0.635	1789	8.028	0.589	52
14.377	0.95	150°	12.975	0.854	36785	9.802	0.644	2203	8.636	0.602	60
14.663	0.95	170°	13.231	0.854	39357	10.014	0.646	2352	8.834	0.606	62

TABLE II: Same as Table I, but for $a = 0.4M$.

p_{init}/M	e_{init}	$\theta_{\text{inc, init}}$	$p_{3:2}/M$	$e_{3:2}$	$T_{3:2}$ (days)	$p_{2:1}/M$	$e_{2:1}$	$T_{2:1}$ (days)	$p_{3:1}/M$	$e_{3:1}$	$T_{3:1}$ (days)
7.304	0.1	10°	6.642	0.082	1771	4.670	0.037	210	3.870	0.025	25
7.832	0.1	30°	7.127	0.083	2203	5.033	0.039	262	4.162	0.027	30
9.460	0.1	60°	8.607	0.084	3984	6.180	0.045	483	5.120	0.034	57
11.253	0.1	85°	10.236	0.085	6964	7.477	0.051	856	6.239	0.042	97
12.001	0.1	95°	10.911	0.085	8596	8.019	0.051	1064	6.713	0.043	121
13.728	0.1	120°	12.478	0.086	13452	9.286	0.055	1688	7.827	0.048	190
15.224	0.1	150°	13.836	0.086	19094	10.390	0.058	2422	8.803	0.052	270
15.708	0.1	170°	14.271	0.086	21226	10.744	0.058	2701	9.117	0.053	301
7.381	0.4	10°	6.693	0.336	1936	4.689	0.158	219	3.887	0.104	23
7.909	0.4	30°	7.175	0.338	2390	5.055	0.167	273	4.183	0.114	29
9.526	0.4	60°	8.654	0.343	4268	6.209	0.192	495	5.155	0.146	49
11.319	0.4	85°	10.286	0.346	7401	7.514	0.215	859	6.296	0.180	76
12.078	0.4	95°	10.962	0.345	9209	8.058	0.215	1078	6.773	0.180	96
13.816	0.4	120°	12.536	0.347	14356	9.335	0.230	1677	7.914	0.203	135
15.323	0.4	150°	13.900	0.348	20383	10.447	0.239	2379	8.914	0.217	179
15.807	0.4	170°	14.338	0.349	22661	10.804	0.241	2644	9.236	0.220	195
7.546	0.7	10°	6.811	0.608	2564	4.749	0.315	258	3.938	0.210	24
8.063	0.7	30°	7.290	0.611	3118	5.122	0.333	316	4.247	0.232	28
9.669	0.7	60°	8.764	0.616	5442	6.290	0.377	552	5.259	0.297	42
11.473	0.7	85°	10.401	0.620	9311	7.614	0.415	912	6.454	0.359	54
12.232	0.7	95°	11.080	0.617	11742	8.160	0.411	1175	6.933	0.353	72
13.992	0.7	120°	12.666	0.620	18249	9.460	0.435	1778	8.132	0.393	90
15.521	0.7	150°	14.046	0.621	25983	10.594	0.448	2493	9.181	0.414	111
16.005	0.7	170°	14.488	0.621	28936	10.959	0.452	2762	9.520	0.420	118
7.744	0.95	10°	6.967	0.850	5115	4.874	0.515	365	4.052	0.354	30
8.250	0.95	30°	7.440	0.851	6120	5.250	0.534	428	4.387	0.394	33
9.845	0.95	60°	8.905	0.854	10475	6.426	0.579	681	5.451	0.485	35
11.660	0.95	85°	10.546	0.856	17951	7.768	0.620	1082	6.703	0.562	39
12.419	0.95	95°	11.229	0.853	22546	8.315	0.610	1437	7.181	0.544	56
14.201	0.95	120°	12.831	0.854	35426	9.643	0.637	2159	8.438	0.591	66
15.752	0.95	150°	14.228	0.855	50934	10.804	0.652	3045	9.535	0.614	80
16.247	0.95	170°	14.677	0.855	56940	11.179	0.656	3384	9.890	0.620	85

TABLE III: Same as Table I, but for $a = 0.7M$.

p_{init}/M	e_{init}	$\theta_{\text{inc, init}}$	$p_{3:2}/M$	$e_{3:2}$	$T_{3:2}$ (days)	$p_{2:1}/M$	$e_{2:1}$	$T_{2:1}$ (days)	$p_{3:1}/M$	$e_{3:1}$	$T_{3:1}$ (days)
5.555	0.1	10°	5.053	0.079	867	3.323	0.019	103	2.680	0.007	13
6.303	0.1	30°	5.737	0.080	1228	3.825	0.025	144	3.057	0.010	17
8.547	0.1	60°	7.788	0.083	2992	5.438	0.039	356	4.403	0.025	42
10.956	0.1	85°	9.971	0.085	6481	7.206	0.049	790	5.953	0.039	91
11.946	0.1	95°	10.858	0.085	8555	7.929	0.050	1054	6.593	0.040	121
14.190	0.1	120°	12.896	0.086	15142	9.592	0.055	1901	8.070	0.048	214
16.115	0.1	150°	14.644	0.086	23311	11.021	0.058	2968	9.343	0.053	331
16.731	0.1	170°	15.201	0.086	26496	11.478	0.059	3386	9.749	0.054	376
5.621	0.4	10°	5.092	0.323	950	3.329	0.081	106	2.682	0.027	14
6.358	0.4	30°	5.775	0.330	1326	3.838	0.107	149	3.065	0.044	18
8.602	0.4	60°	7.824	0.340	3180	5.460	0.167	369	4.424	0.107	41
11.011	0.4	85°	10.012	0.346	6838	7.237	0.207	797	5.997	0.167	75
12.001	0.4	95°	10.902	0.345	9127	7.963	0.210	1072	6.643	0.170	100
14.267	0.4	120°	12.950	0.347	16117	9.639	0.230	1889	8.155	0.202	154
16.203	0.4	150°	14.708	0.349	24847	11.081	0.242	2906	9.461	0.220	217
16.830	0.4	170°	15.269	0.349	28253	11.541	0.244	3301	9.879	0.225	239
5.753	0.7	10°	5.190	0.597	1266	3.346	0.164	114	2.687	0.053	13
6.479	0.7	30°	5.866	0.605	1709	3.876	0.222	166	3.086	0.090	19
8.701	0.7	60°	7.908	0.616	3976	5.521	0.337	414	4.484	0.223	41
11.132	0.7	85°	10.105	0.620	8469	7.320	0.404	845	6.124	0.339	57
12.133	0.7	95°	11.002	0.617	11526	8.051	0.402	1172	6.779	0.336	81
14.421	0.7	120°	13.072	0.621	20388	9.759	0.436	1998	8.369	0.392	103
16.401	0.7	150°	14.852	0.622	31606	11.231	0.453	3032	9.742	0.420	132
17.028	0.7	170°	15.420	0.622	36025	11.702	0.457	3435	10.182	0.427	143
5.918	0.95	10°	5.331	0.856	2719	3.391	0.292	140	2.697	0.084	15
6.622	0.95	30°	5.991	0.855	3399	3.959	0.395	218	3.127	0.152	22
8.833	0.95	60°	8.016	0.856	7520	5.622	0.535	524	4.601	0.380	47
11.275	0.95	85°	10.224	0.858	16165	7.448	0.611	987	6.332	0.541	43
12.287	0.95	95°	11.129	0.854	21898	8.184	0.600	1427	6.992	0.523	66
14.619	0.95	120°	13.225	0.855	39459	9.933	0.638	2417	8.666	0.590	76
16.632	0.95	150°	15.032	0.856	62016	11.445	0.657	3706	10.107	0.620	96
17.270	0.95	170°	15.610	0.856	71082	11.929	0.662	4214	10.570	0.628	104

TABLE IV: Same as Table I, but for $a = 0.9M$.

p_{init}/M	c_{init}	$\theta_{\text{inc, init}}$	$N_{\theta,3:2}$	$N_{r,3:2}$	$N_{\theta,2:1}$	$N_{r,2:1}$	$N_{\theta,3:1}$	$N_{r,3:1}$
11.297	0.1	10°	1827.94	1218.62	930.84	465.42	323.97	107.99
11.363	0.1	30°	1838.92	1225.95	936.91	468.45	326.14	108.71
11.583	0.1	60°	1872.76	1248.51	955.57	477.79	332.78	110.93
11.825	0.1	85°	1910.84	1273.89	976.54	488.27	340.22	113.41
11.935	0.1	95°	1927.01	1284.68	985.45	492.72	343.41	114.47
12.177	0.1	120°	1965.02	1310.01	1006.34	503.17	350.80	116.93
12.397	0.1	150°	1998.72	1332.48	1024.86	512.43	357.35	119.12
12.463	0.1	170°	2009.64	1339.76	1030.86	515.43	359.47	119.82
11.385	0.4	10°	1795.66	1197.10	936.83	468.42	312.82	104.27
11.451	0.4	30°	1806.08	1204.05	942.73	471.37	314.64	104.88
11.671	0.4	60°	1838.33	1225.56	960.83	480.42	320.26	106.75
11.913	0.4	85°	1874.19	1249.46	980.84	490.42	326.12	108.71
12.034	0.4	95°	1891.08	1260.72	990.38	495.19	329.75	109.92
12.276	0.4	120°	1926.99	1284.66	1010.35	505.17	335.53	111.84
12.485	0.4	150°	1959.24	1306.16	1028.34	514.17	340.88	113.63
12.562	0.4	170°	1969.80	1313.20	1034.17	517.09	342.64	114.21
11.572	0.7	10°	1742.62	1161.75	946.20	473.10	284.55	94.85
11.649	0.7	30°	1752.20	1168.13	951.58	475.79	285.79	95.26
11.869	0.7	60°	1781.53	1187.69	968.11	484.06	289.31	96.44
12.111	0.7	85°	1813.42	1208.95	985.49	492.74	291.96	97.32
12.221	0.7	95°	1830.97	1220.65	996.76	498.38	296.72	98.91
12.474	0.7	120°	1863.26	1242.17	1014.20	507.10	299.42	99.81
12.683	0.7	150°	1892.85	1261.90	1030.74	515.37	302.55	100.85
12.760	0.7	170°	1902.64	1268.42	1036.13	518.07	303.68	101.23
11.803	0.95	10°	1707.47	1138.31	945.63	472.81	242.47	80.82
11.880	0.95	30°	1716.08	1144.05	950.38	475.19	243.25	81.08
12.100	0.95	60°	1742.52	1161.68	964.87	482.43	245.22	81.74
12.342	0.95	85°	1770.70	1180.47	978.79	489.40	245.45	81.82
12.452	0.95	95°	1788.46	1192.30	992.34	496.17	251.34	83.78
12.705	0.95	120°	1817.11	1211.40	1006.51	503.26	251.75	83.92
12.925	0.95	150°	1844.22	1229.48	1021.19	510.59	253.56	84.52
12.991	0.95	170°	1853.01	1235.34	1025.96	512.98	254.08	84.69

TABLE V: Number of θ and r oscillations spent near resonance as a function of initial orbit parameters for spin $a = 0.1M$, defined by Eq. (2.18). All values are for $M = 10^6 M_\odot$, $\mu = 1 M_\odot$; these results can be extrapolated to other masses using the rule that $N_{\theta,r} \propto \sqrt{M/\mu}$ [Eq. (3.15)]. Notice that the number of oscillations near each resonance is quite large: ~ 100 in the shortest cases, and ~ 2000 in the longest ones.

p_{init}/M	c_{init}	$\theta_{\text{inc, init}}$	$N_{\theta,3:2}$	$N_{r,3:2}$	$N_{\theta,2:1}$	$N_{r,2:1}$	$N_{\theta,3:1}$	$N_{r,3:1}$
9.427	0.1	10°	1548.67	1032.45	776.52	388.26	268.49	89.50
9.713	0.1	30°	1593.30	1062.20	801.38	400.69	277.47	92.49
10.604	0.1	60°	1729.99	1153.33	877.14	438.57	304.71	101.57
11.594	0.1	85°	1882.99	1255.32	961.58	480.79	334.85	111.62
12.012	0.1	95°	1947.76	1298.51	997.32	498.66	347.73	115.91
12.991	0.1	120°	2099.66	1399.78	1081.05	540.53	377.50	125.83
13.849	0.1	150°	2233.88	1489.25	1155.01	577.51	403.78	134.59
14.124	0.1	170°	2277.32	1518.21	1178.95	589.47	412.27	137.42
9.515	0.4	10°	1529.13	1019.42	786.66	393.33	266.04	88.68
9.801	0.4	30°	1570.73	1047.15	810.73	405.36	274.16	91.39
10.681	0.4	60°	1699.28	1132.85	884.09	442.05	298.16	99.39
11.671	0.4	85°	1842.97	1228.65	964.62	482.31	322.46	107.49
12.100	0.4	95°	1910.21	1273.47	1002.91	501.45	336.62	112.21
13.079	0.4	120°	2054.55	1369.70	1083.13	541.56	359.76	119.92
13.937	0.4	150°	2184.31	1456.20	1155.10	577.55	380.60	126.87
14.223	0.4	170°	2226.53	1484.36	1178.41	589.21	387.30	129.10
9.702	0.7	10°	1499.32	999.55	809.12	404.56	258.25	86.08
9.977	0.7	30°	1535.56	1023.70	830.71	415.35	263.82	87.94
10.868	0.7	60°	1649.91	1099.94	896.71	448.36	279.47	93.16
11.858	0.7	85°	1777.12	1184.74	966.22	483.11	290.31	96.77
12.287	0.7	95°	1847.39	1231.59	1011.20	505.60	308.72	102.91
13.266	0.7	120°	1977.83	1318.56	1081.91	540.96	318.66	106.22
14.135	0.7	150°	2098.99	1399.33	1148.54	574.27	330.38	110.13
14.421	0.7	170°	2138.64	1425.76	1170.24	585.12	334.21	111.40
9.911	0.95	10°	1486.71	991.14	827.67	413.84	235.40	78.47
10.197	0.95	30°	1518.30	1012.20	845.36	422.68	237.80	79.27
11.077	0.95	60°	1619.26	1079.51	901.09	450.55	244.46	81.49
12.078	0.95	85°	1731.22	1154.15	955.86	477.93	243.91	81.30
12.507	0.95	95°	1802.38	1201.58	1009.73	504.87	267.11	89.04
13.497	0.95	120°	1919.46	1279.64	1067.84	533.92	267.07	89.02
14.377	0.95	150°	2031.41	1354.27	1127.47	563.74	273.04	91.01
14.663	0.95	170°	2068.15	1378.77	1147.02	573.51	275.07	91.69

TABLE VI: Same as Table V, but for $a = 0.4M$. As in the $a = 0.1M$ case, the number of oscillations spent near each resonance is quite large.

p_{init}/M	c_{init}	$\theta_{\text{inc, init}}$	$N_{\theta,3:2}$	$N_{r,3:2}$	$N_{\theta,2:1}$	$N_{r,2:1}$	$N_{\theta,3:1}$	$N_{r,3:1}$
7.304	0.1	10°	1250.91	833.94	610.35	305.18	208.82	69.61
7.832	0.1	30°	1331.61	887.74	656.36	328.18	225.65	75.22
9.460	0.1	60°	1575.42	1050.28	792.41	396.21	274.98	91.66
11.253	0.1	85°	1845.88	1230.59	941.51	470.76	328.24	109.41
12.001	0.1	95°	1960.00	1306.66	1004.36	502.18	350.79	116.93
13.728	0.1	120°	2226.87	1484.58	1151.47	575.74	403.04	134.35
15.224	0.1	150°	2461.90	1641.26	1281.02	640.51	448.97	149.66
15.708	0.1	170°	2537.83	1691.89	1322.86	661.43	463.78	154.59
7.381	0.4	10°	1248.69	832.46	623.44	311.72	212.42	70.81
7.909	0.4	30°	1320.58	880.38	668.19	334.09	229.00	76.33
9.526	0.4	60°	1545.63	1030.42	800.30	400.15	275.55	91.85
11.319	0.4	85°	1799.60	1199.73	942.92	471.46	320.13	106.71
12.078	0.4	95°	1918.26	1278.84	1009.92	504.96	343.97	114.66
13.816	0.4	120°	2173.66	1449.10	1151.51	575.75	384.48	128.16
15.323	0.4	150°	2402.57	1601.72	1277.81	638.90	419.76	139.92
15.807	0.4	170°	2476.78	1651.18	1318.61	659.31	430.88	143.63
7.546	0.7	10°	1249.07	832.71	661.42	330.71	224.99	75.00
8.063	0.7	30°	1306.00	870.67	700.63	350.31	240.21	80.07
9.669	0.7	60°	1499.00	999.33	817.77	408.88	275.58	91.86
11.473	0.7	85°	1724.10	1149.40	940.78	470.39	295.16	98.39
12.232	0.7	95°	1848.31	1232.20	1018.83	509.42	324.80	108.27
13.992	0.7	120°	2082.42	1388.28	1145.27	572.63	341.14	113.71
15.521	0.7	150°	2298.83	1532.55	1262.88	631.44	359.29	119.76
16.005	0.7	170°	2369.21	1579.47	1300.96	650.48	364.98	121.66
7.744	0.95	10°	1263.91	842.61	720.75	360.37	259.37	86.46
8.250	0.95	30°	1308.75	872.50	743.76	371.88	263.68	87.89
9.845	0.95	60°	1473.91	982.61	831.54	415.77	263.92	87.97
11.660	0.95	85°	1672.12	1114.74	926.52	463.26	251.94	83.98
12.419	0.95	95°	1797.82	1198.55	1019.35	509.68	290.65	96.88
14.201	0.95	120°	2010.42	1340.28	1125.18	562.59	286.82	95.61
15.752	0.95	150°	2212.45	1474.97	1231.09	615.55	294.38	98.13
16.247	0.95	170°	2278.52	1519.02	1265.56	632.78	297.07	99.02

TABLE VII: Same as Table V, but for $a = 0.7M$. Again we see many oscillations near each resonance.

p_{init}/M	c_{init}	$\theta_{\text{inc, init}}$	$N_{\theta,3:2}$	$N_{r,3:2}$	$N_{\theta,2:1}$	$N_{r,2:1}$	$N_{\theta,3:1}$	$N_{r,3:1}$
5.555	0.1	10°	1040.54	693.69	496.24	248.12	171.77	57.26
6.303	0.1	30°	1146.72	764.48	556.67	278.34	192.09	64.03
8.547	0.1	60°	1465.33	976.89	733.84	366.92	255.86	85.29
10.956	0.1	85°	1816.70	1211.14	926.27	463.14	323.75	107.92
11.946	0.1	95°	1964.41	1309.61	1007.32	503.66	352.56	117.52
14.190	0.1	120°	2308.88	1539.26	1196.90	598.45	419.66	139.89
16.115	0.1	150°	2611.50	1741.00	1363.62	681.81	478.63	159.54
16.731	0.1	170°	2709.19	1806.12	1417.44	708.72	497.64	165.88
5.621	0.4	10°	1059.72	706.48	504.33	252.16	172.90	57.63
6.358	0.4	30°	1145.20	763.47	565.87	282.93	194.22	64.74
8.602	0.4	60°	1432.90	955.27	741.04	370.52	259.49	86.50
11.011	0.4	85°	1764.06	1176.04	926.30	463.15	319.71	106.57
12.001	0.4	95°	1918.03	1278.69	1012.30	506.15	349.15	116.38
14.267	0.4	120°	2249.57	1499.72	1195.52	597.76	401.35	133.78
16.203	0.4	150°	2545.56	1697.04	1358.24	679.12	445.64	148.55
16.830	0.4	170°	2641.47	1760.98	1410.78	705.39	459.60	153.20
5.753	0.7	10°	1098.79	732.53	531.67	265.84	176.33	58.78
6.479	0.7	30°	1147.10	764.73	596.76	298.38	201.32	67.11
8.701	0.7	60°	1382.96	921.97	759.38	379.69	271.07	90.36
11.132	0.7	85°	1678.84	1119.23	921.04	460.52	303.58	101.19
12.133	0.7	95°	1840.54	1227.03	1020.42	510.21	337.85	112.62
14.421	0.7	120°	2147.35	1431.57	1185.83	592.92	357.66	119.22
16.401	0.7	150°	2429.46	1619.64	1337.90	668.95	378.86	126.29
17.028	0.7	170°	2521.06	1680.71	1387.04	693.52	385.64	128.55
5.918	0.95	10°	1144.25	762.83	617.07	308.54	184.00	61.33
6.622	0.95	30°	1165.19	776.80	672.55	336.28	219.48	73.16
8.833	0.95	60°	1358.49	905.66	779.79	389.89	292.49	97.50
11.275	0.95	85°	1620.62	1080.41	903.79	451.89	266.61	88.87
12.287	0.95	95°	1784.38	1189.59	1021.31	510.65	312.28	104.09
14.619	0.95	120°	2065.73	1377.16	1161.82	580.91	302.29	100.76
16.632	0.95	150°	2330.75	1553.83	1299.25	649.62	309.27	103.09
17.270	0.95	170°	2417.14	1611.43	1343.78	671.89	312.11	104.04

TABLE VIII: Same as Table V, but for $a = 0.9M$. Again we see many oscillations near each resonance.